Polyimide-Based Flexible Multi-Electrode Arrays: Synthesis, Microfabrication, and *in-vivo* Validation

Kshitij Kumar[*‡], Kaustubh Deshpande[#‡], Naveen Kalur[#], Garima Chauhan[*]
Deepti Chugh[*], Subramaniam Ganesh[*], Arjun Ramakrishnan[*#]

[*]Department of Biological Sciences & Bioengineering,
Indian Institute of Technology Kanpur, Uttar Pradesh, India, 208016

Eywa Neuro PLC, India

‡ Equal Contribution

***Abstract*—Thin film neural microelectrodes are popularly being used in brain-computer interfaces and tools for neurosurgical interventions [8]. Among the various thin films used, polyimide stands out as an excellent material for substrate passivation due to its chemical inertness, biocompatibility, mechanical flexibility, and superior dielectric properties. While polyimide is extensively used as a substrate in thin film neural interfaces, the lack of availability of a clinical-grade polyimide limits their use in human clinical applications. This paper presents a comprehensive solution by developing an ISO-10993-11-approved polyamic acid for fabricating thin-film polyimide microelectrodes. Benchtop tests and in-vivo experiments in anesthetized mice demonstrate the potential of this synthesized polyamic acid and microfabrication processes for commercialization in clinical settings, particularly for brain-computer interfaces and invasive neural microelectrodes.**

***Index Terms*—Polyimide, Neural Probes, MEMS.**

I. Introduction

Invasive neural interfaces offer valuable insights into the nervous system's function by enabling direct communication with neurons. They are widely used in clinical and commercial applications, such as electroencephalogram (EEG), brain-computer interfaces, and intervention therapies. Invasive neural interfaces enable neurosurgical interventions for disorders like epilepsy, depression, Parkinson's, urinary incontinence, and blindness [22] . However, they face challenges in channel scaling, chronic longevity, reduced foreign body response, and meeting regulatory limits set by the Food and Drug Administration (FDA) [14]. Addressing these issues through ongoing research is essential to ensure their safety, long-term functionality, and suitability for commercial use, with strict adherence to FDA guidelines being particularly important.

To study the nervous system, invasive neural interfaces must be developed that record from large populations of neurons to single neurons. Among the various activities recorded by invasive neural interfaces, Local field potentials (LFP) and Extracellular Action Potentials (referred to as Single Units) hold significant promise for research and clinical applications. LFPs are low-frequency oscillations, ranging up to 500 Hz, that reflect the coordinated activity of large populations of neurons, while single units provide information about the firing patterns of individual neurons [22]. Studies utilizing LFPs in the hippocampus for memory formation and retrieval, and single units in the prefrontal cortex for decision-making processes, have demonstrated the importance of decoding these signals for understanding behavior and cognition [16]. The data obtained from these recordings can ultimately be used to study brain function and dysfunction, as well as to develop new therapies for neurological disorders such as epilepsy and Parkinson's disease. Real-time decoding of LFPs and single units can also be used to develop brain-computer interfaces (BCIs) that enable individuals with paralysis to control prosthetic limbs or devices using their thoughts. Accurate decoding of LFPs and single units requires a series of software-controlled filters along with neural interfaces of appropriate electrode dimensions. However, challenges remain, such as variability of neural signals over time and the need for long-term stability of implanted electrodes.

Neural interfaces have traditionally used microwires made of tungsten, gold, or platinum-iridium [13]. These devices have electrode diameters ranging from 20 μm to 100 μm and provide a good signal-to-noise ratio (SNR). However, assembly limitations, scaling, and potential surgical trauma hinder their widespread use. Micro-Electro-Mechanical Systems (MEMS) technology was used to overcome these shortcomings, allowing for high channel count neural interfaces that can be miniaturized and cause less tissue damage. Silicon microelectrode arrays were one of the first MEMS-based neural interfaces, gaining attention due to their small size, sharp tips, and ease of implantation. But because of the tissue damage caused by their stiffness, brittleness, and lack of biocompatibility, their use in clinical applications is limited [19]. Researchers are now developing flexible substrates that better match the mechanical properties of brain tissue, resulting in less severe foreign body reactions and reduced tissue damage from micromotion [23]. The development of polymer-based neural interfaces made of parylene [21], polyimide [20], SU8 [1], and Liquid Crystal Polymer [11] has led to a surge in the adoption of flexible neural interfaces, with major BCI companies like Neuralink [2], Precision Neuroscience, and Neuro-One Technologies making breakthrough commercial technologies. Flexible substrates also offer more precise and accurate recordings of long-term neural activity, and as the field advances, they have the potential to become the standard for invasive neural interfaces.

The size of the neural interface is crucial for its flexibility and minimizing surgical trauma during insertion [18]. Research studies have focused on improving softness and reducing Young's modulus of polymers, along with miniaturizing

the form factor without losing desired properties [12]. Novel lithography techniques like stepper lithography and electron-beam lithography can help achieve this. However, process limitations prevent certain polymers from being scaled down further. In this regard, Polyimide is a popular choice due to its excellent dielectric features, chemical and radiation inertness, mechanical strength, durability, high-temperature resistance, flexibility and, most importantly, because it can be spun into thin films of less than 10 μm [5]. Polyimide neural interfaces have been commercialized by companies like Neuralink [2] and Neuro One Technologies [10], and have also been used in life science and acute electrophysiology research.

Polyimide thin films are synthesized using polyamic acid, which is spin-coated and cured at high temperatures to imidize it into thin films [7]. This process allows thermal or chemical imidization, releasing H_2O and forming aromatic rings with chemical inertness. Two popular polyamic acids for thin film neural interface fabrication are Pyralin 2610/2611 by HD Microsystems and U-Varnish by UBE Industries [17]. These electronic-grade polyamic acids, however, are not widely used in human medical research. Polyamic acids are synthesized through a two-stage reaction between diamine and dianhydride in a polar aprotic solvent. The properties of the polyimide change depending on the monomers used. Photosensitive polyimides can be synthesised for patterning, but are more moisture sensitive and limited in in-vivo usage [8]. Diphenyl dianhydride (BPDA) and p-phenylenediamine (p-PPD) are popular monomer options due to their low moisture absorption, stability, and biocompatibility. This chemistry has been used to create neural interfaces and has been extensively tested for their biocompatibility [15]. However, the lack of availability of a clinical-grade polyimide limits the use of thin film polyimide electrodes in human clinical applications. By synthesizing our own polyamic acid chemistry and microfabricating neural interfaces from it, we aim to demonstrate an end-to-end neural interface solution that holds true potential for commercial viability.

In this study, we achieve the following objectives 1. BPDA: p-PPD-based polyimide synthesis. 2. Characterization of the surface roughness, temperature stability, chemical inertness, and insulation properties of the polyimide film. 3. Micro-fabrication of (4-channel, 10 μm thick) depth and surface neural microelectrode arrays. 4. Benchtop electrochemical characterisation. 5. Surface and intracortical implantation of the arrays. 6. Demonstration of high quality neural activity:isolated single units and quantified signal-to-noise ratio. 7. Successful clearance of acute systemic toxicity tests in mice using the ISO-10993-11 standard. In conclusion, these results recommend the use of the synthesised polyimide films as a potential clinical-grade thin-films candidate for neural interfaces.

II. Materials and Methods

A. Polyamic acid synthesis

The production of polyamic acid involved an equimolar polycondensation reaction between s-BPDA (Merck, India) and p-PPD (Merck, India) in a polar Di-methyl-acetamide (DMAc) solvent (Leo Chemo Plast Pvt. Ltd, India). A water condenser with a nitrogen gas purge setup at the top was attached to a 500 ml capacity, four-necked round-bottomed flask. The vessel was also equipped with an agitator and a thermocouple. Prior to adding any reagents, the vessel was completely purged with nitrogen. The flask was first filled with 250 gm of DMAc and then heated to 30°C. 0.078 moles of p-PPD were then added, and the mixture was stirred while being heated to 90°C and maintained there for two hours to achieve complete dissolution. The solution was then cooled to 50°C while being continuously stirred. s-BPDA was then added in an equimolar ratio to p-PPD, and the mixture was stirred for three hours. The solution was then cooled below 30°C and stirred for 7 to 8 hours until a viscous yellow solution was obtained. To filter out any coarse or unreacted particles, the polyamic acid was filtered through a Grade 41 Whatman filter paper with the help of a vacuum and a Buchner funnel. Finally, the polyamic acid was degassed in a vacuum for 24-48 hours to remove any entrapped gasses.

B. Material Characterisation

The thermal imidization properties and curing properties of n=3 independently synthesized polyamic acids were studied using thermogravimetric analysis (TGA) and differential scanning calorimetry (DSC).TGA can be used to determine mass change in a polyamic acid sample as its temperature rises linearly [24]. Knowledge about the thermal stability and curing of the polyamic acid could be extrapolated from this study. To confirm the temperature at which the polyamic acid was imidized, a differential scanning calorimetry (DSC) analysis was conducted. This method quantifies the energy required by the polyamic acid to increase its temperature, as a function of temperature. Based on these studies, a curing process for the polyamic acid was developed to attain a high degree of imidization.

The curing recipe was verified by running Fourier Transform Infra-Red Spectroscopy (FTIR) on the polyamic acid and on cured polyimide films. A total of 5 cured polyimide samples were used to confirm their FTIR spectra. The absorption bands of amide and imide peaks on FTIR spectra are used to confirm successful synthesis and imidization. Based on [6], we verified the presence of N-H, C=C, and C=O amide and imide peaks on the polyamic acid and the cured polyimide respectively.

Additionally, TGA was run on the polyamic acid sample with the verified curing recipe conditions, and the recorded change in weight was used as a metric that represented the degree of imidization. Polyamic acid when cured imidizes with the release of the solvent (DMAc) and H_2O. When imidization is complete, little to no change in weight is recorded.

Test structures of metal lines that were electrically shorted between themselves and encapsulated with polyimide were fabricated. If the polyimide gets compromised, the structures are exposed, causing a drop in impedance when tested with electrochemical impedance spectroscopy in saline. The test structures were soaked in different cleanroom chemicals to

test for polyimide's chemical inertness. Fig 1 (A). shows the test structure design.

Finally, spun polyimide films were tested for pinholes and surface roughness using Atomic Force Microscopy (AFM). The AFM probe was used to scan areas on multiple spun polyimide films to detect variations in surface profile and to check for the presence or absence of pinholes.

To evaluate its suitability as a long-term substrate for neural interfaces, a key criterion is a substrate's low moisture absorption. In this study, a polyimide film sample's moisture uptake was assessed using a TGA microbalance. Initially, the dry weight of the polyimide film was measured as a baseline. Subsequently, the film was soaked in deionized water for 24 hours and then dried with nitrogen gas. The TGA machine further dehydrated the film at 100°C for 10 minutes to eliminate any absorbed moisture. The moisture uptake percentage was determined as the weight increase of the polyimide sample compared to its initial weight.

C. Microfabrication Process

The microfabrication of neural microelectrodes was performed with a two-mask process as shown in Fig 1 (B). First, polyamic acid was spin-coated on an RCA-cleaned silicon wafer at 5000 rpm. The polyamic acid was then soft baked at 100°C for 5 minutes followed by 120°C for 5 minutes on a hotplate. To cure the polyamic acid and imidize it into polyimide, the wafers were loaded in a furnace and cured at a final temperature of 350°C using nitrogen as an ambient gas. The polyimide was then roughened using O_2 plasma in a plasma asher (PDC-32G-2, Harrick Plasma Systems). Next, a bilayer liftoff pattern using S1813 positive photoresist(Microresist Technology) and LOR3B(Kayaku Advanced Materials) lift-off resist was patterned using hard-contact photolithography (EVG Double Sided Aligner). The channels have a 5 μm space and trace width. A stack of Titanium (20 nm), Platinum (50 nm), Gold (200 nm), Platinum (50 nm), and Titanium (20 nm) was then deposited using a sputter deposition tool (Multi-Target Sputter, AJA Systems). The metal layers are lifted off in Remover PG (Kayaku Advanced Materials) to define the traces, electrode pads, and bondpads. After liftoff, the wafers were passed through an O_2 plasma descum in a plasma asher to roughen the underlying polyimide layer, as well as to etch away any undissolved photoresist. The second layer of polyimide was then spun and cured as discussed previously. Each polyimide layer stack was 5 μm in thickness. To pattern the electrodes, bondpads, and outline, we made use of an aluminium (Al) hard mask. First, 100 nm aluminium was deposited using sputter deposition (Multi-Target Sputter, AJA Systems). The Aluminium was then patterned with S1813 photoresist and was wet etched in Type-A aluminium etchant(Transense). Finally, polyimide was etched using an O_2 plasma in a plasma asher to etch the device outline and open the electrodes and bondpads. The aluminium was then etched away by soaking the wafers in Type A aluminium etchant. The devices were finally released off the wafer by soaking them in isopropanol and peeling them with fine-tip tweezers. Fig 1 (C). shows the designs of the invasive neural interfaces. The bondpads were fabricated with through-holes and were directly soldered to an electronic interface board with 1.27 mm male pin connectors.

D. Impedance Characterization

The impedance of the fabricated arrays was characterized using a Metrohm Potentiostat (STAT-I-400S) for electrochemical impedance spectroscopy (EIS) studies. A 3-electrode setup was used, with a silver/silver chloride electrode as a reference electrode and a 0.5 mm diameter platinum wire as a counter electrode. 1X PBS (Phosphate buffered saline) (Merck, India) was used as a solution medium as a way to mimic the cerebral spinal fluid in the brain. A sinusoidal signal of 50 mV was applied from 100 Hz to 10 kHz with 3 points per decade. The potential was applied between the electrode site and the reference electrode, and the current was measured between the electrode site and the counter electrode.

E. Surgical Protocol and Animal Preparation

Fig 1 (D). shows an illustration of the surgical setup. All experiments were performed in accordance with the institutional animal ethics committee (IAEC) guidelines after obtaining approvals for the protocols (IAEC project number: IITK/IAEC/2021/1137). The study employed a total of two transgenic C57BL6 mice (Laforin knockout mouse model of epilesy) across 20 recording sessions. The flexible electrode tip was hardened using a hydrophilic polyether compound before the animal was prepared for surgery. Polyethylene glycol (PEG) (Merck, India) was gently dip-coated on the electrode tip after being carefully melted on a hot plate at 70°C. The procedure was repeated several times until the required stiffness was obtained. Aseptic techniques were followed while performing stereotactic implantation surgery. Mice were anesthetized with inhaled isoflurane (5% Induction, 1-1.5% maintenance in 100% oxygen). The level of anesthesia was monitored using a gentle toe pinch withdrawal reflex. Throughout the surgical process, the anesthetic depth was re-evaluated every 10 to 30 minutes. A heating pad with a thermostat was used to provide thermoregulation, which was monitored at all times during the procedure. Subcutaneous injection of 0.1 mg/kg lidocaine was administered as a local anaesthetic. With a scalpel blade, a primary incision was made that extended from the area between the eyes to the cerebellum. The Coronal and Sagittal sutures were identified, and the reference point bregma was located using a surgical microscope. A 1 mm × 1 mm craniotomy was performed using an electric micro-drill with a 1 mm drill bit. Care was taken to stop the drill bit before it penetrated through meningeal membranes or blood vessels. The bone flap was then carefully elevated from the underlying dura. Physiological saline solution (0.9% Nacl) was constantly applied to the brain surface to avoid drying of brain tissue during recording. A robotic stereotaxic equipment (Neurostar, GMBH, Germany) was used to guide the placement of a depth probe, a 5 mm long, 4-channel polyimide neural microelectrode with

400 μm^2 Platinum sites, in the right somatosensory cortex (coordinates: AP: -0.9, ML: +3, DV: -1.5). Another 9 mm x 3 mm craniotomy covering the frontal and occipital regions was performed in the left hemisphere. The cortical surface was in contact with the μECoG polyimide electrode that was 7.5 mm long and had four platinum electrodes with an area of 0.64 mm^2. The mouse brain atlas served as a reference for positioning the electrodes, which was achieved together with the help of the robotic stereotaxic arm. *In-vivo* electrophysiological recordings were acquired and analyzed.

F. Electrophysiological recordings (Acquisition & Analysis)

For all of the animals used in this study, electrophysiological data was acquired using the Intan RHS stim/recording system (Intan technologies). For the purpose of preventing signal loss during data transmission, neuronal data was captured inside a Faraday cage in addition to using an RHS32 low noise amplifier headstage. The signals were digitized at 30 kHz. A notch filter with a cutoff frequency of 50 Hz was used to filter out any electrical noise signals at this frequency for online real-time visualization. Real-time filtering, using a band pass filter (300-6000 Hz), improved the ability to gauge neuronal activity during the experiment and aided in determining probe insertion depth, again only for online real-time visualization. During data acquisition, a hardware reference was employed to further minimize common mode noise in the recordings.

G. Neural Data Analysis

Surface μECoG arrays were placed on the left cerebral cortex, while depth array was implanted in the right somatosensory cortex. We present data from 20 individual sessions, each lasting 10 minutes, from 2 animals. Fig 4 (B) shows a Local Field Potential (LFP) recording of a sample session. The channels comprising μECoG and depth array recordings were separated into two groups. To create time-frequency plots and the spectrograms, the two groups were examined independently using spike interface (v 0.97.1) [3]. The raw, unfiltered recording of the arrays is shown in Fig. 4 (A). Wide-band neuronal data was first filtered using a band pass filter (for μECoG; 0.3–300 Hz and for depth probe, 300–6000 Hz) to visualize the time-frequency plots and for further analysis. Additionally, a 50 Hz notch filter was used to remove line noise from the signals. A central median reference (CMR) method was used to re-reference the recording at the global reference. The data was then normalised using the Z-score value and whitened to remove extraneous artifacts.

To assess signal quality we examined the following quality metrics [3]:

1. Signal-to-noise ratio (SNR) which measures the ratio of the maximum amplitude of the mean spike waveform to the standard deviation of the background noise.

2. To understand the changes in firing rate over the entire recording session, we measured the presence ratio. It is used to identify incomplete units or highly selective units. It calculates the fraction of time when a unit is spiking which typically ranges from 0 to 0.99.

3. Following spike sorting, the isolation distance (ID), which measures how well one cluster is segregated from other clusters recorded on the same electrode, was calculated.

4. Other parameters like average firing rate per session (total number of spikes by the duration of the recording), inter-spike interval (ISI) violation ratio as described by [9] and mean number of spikes per session were also computed and reported in the results section.

To test for differences between the surface and the depth array, statistical significance was assessed using the Mann–Whitney U test.

III. Results

A. Polyamic Acid Synthesis

The polyamic acid synthesized had an inherent viscosity of 2.0 dl/g as measured by an Ubbelohde viscometer . The polyamic acid was characterized for its film properties by spin coating on a silicon wafer and checking for the presence of pinholes or impurities. Fig 2 (A). shows a spin-coated layer of polyamic acid that was soft-baked. Optical microscopy confirmed that there were no pinholes or contaminants present on the surface of this film. These results indicate that the polyamic acid did not outgas during either spin coating or soft baking. The synthesized polyamic acid can be diluted with DMAc to create thinner layers of polyimide, enabling further miniaturization of neural interfaces.

B. Differential Scanning Calorimetry Analysis (DSC)

Fig 2 (B). illustrates the exotherm obtained by heating the polyamic acid to 400°C at a ramp rate of 10°C/min, using a Differential Scanning Calorimetry Tool (DSC7020, Hitachi). From the exotherm, we observe one major transition around 160°C, which correlates to the evaporation of DMAc from the polyamic acid. The exotherm does not have any other major thermal transitions and has a non-reversing heat flow. This goes to suggest that cyclization, imidization, and loss of solvent continue up to 400°C.

C. Thermogravimetric Analysis (TGA)

Thermal analysis was conducted using a thermogravimetric analyser (NEXTA STA300, Hitachi) up to 400°C, with temperature ramping at 4°C/min. A TGA response curve of one polyamic acid sample is shown in Fig.2 (C). The experiment was conducted in 30-minute isothermal intervals at 150°C, 250°C, 350°C, and 400°C. The weight loss from 160°C to 400°C was continuous, with 13.9% weight remaining at 250°C, 12.4% at 350°C, and 12.3% at 400°C. This weight loss corresponds to the loss of H_2O during cyclization and imidization. As the temperature increased from 250°C to 400°C, the rate of weight change decreased, and beyond 350°C, the weight change was negligible, indicating that most imidization was complete. The curing recipe was adopted, consisting of a 150°C isothermal for 30 minutes, followed by a 250°C isothermal, and a 350°C isothermal for 30 minutes each, with in-between ramp steps at a rate of 4°C/min. A final cool-down step was performed at a rate of 5°C/min until

a minimum temperature of 75°C is reached. We can also confirm that the solid weight % in the polyamic acid was 12.3%. This result also showed that cured polyimide could withstand the high temperatures that are often encountered during microfabrication processes.

D. Chemical Inertness

Test structures were soldered to an electronic interface board terminating in 1.27 mm connector pins. The solder connections were potted in epoxy to ensure that connections were not affected by moisture or vapors of any of the test chemicals. Using micromanipulators, the distal end (8.5 mm) of the test structures was soaked for 48 hours at room temperature (27°C) in the following chemicals: a.) PRS 2000 (JT Baker) b.) Type A Aluminium etchant (Transene) c.) PBS 1X (Merck, India) d.) Hydrocholric acid (JT Baker) e.) IPA (JT Baker). After the soak, they were rinsed with deionised water and their impedance was tested with electrochemical impedance spectroscopy in PBS 1X from 100 Hz to 100 kHz. The polyimide insulation was not compromised, according to test results for n=5 samples in each chemical, and all readings indicated no change in electrical impedance. Optical examination further demonstrated that the connections were secure and that neither an open nor a break had occurred during the experiment or handling. According to this study, the polyimide film has excellent chemical inertness after curing.

E. Fourier Transform Infra-Red Spectroscopy (FTIR)

FTIR was used to analyze the polyamic acid and cured polyimide film's spectral fingerprints for various chemical species (Vertex 80, Bruker). Fig 2 (D). shows the transmission spectra of polyamic acid and cured polyimide samples. We can observe peaks in the polyamic acid spectrum between 2900 and 3200 cm^{-1} that correspond to N-H stretch bonds. Around 1653 cm^{-1} is the amide I's C=O carbonyl stretch. The polyimide exhibits imide I peak (C=O stretch) at 1768 cm^{-1}, C-N stretch at 1378 cm^{-1}, C-H bend at 1123 cm^{-1}, and C=O bend at 736 cm^{-1} after curing. These findings do imply that the synthesized polyamic acid and cured polyimide have a transmission spectra that are similar to those reported in [6].

F. Surface Roughness

Atomic force microscopy (AFM), as opposed to surface profilometry, can measure surface roughness with a resolution as low as a picometer. Additionally, presence of pinholes can be detected using AFM. By performing numerous smaller AFM scans, we were able to cover a total area of 20 mm by 20 mm (MFP3D Origin, Oxford Instruments). Samples from 4 wafers of 5 μm thick polyimide films were scanned at 1 Hz with 256 points per scan. A 5 μm polyimide film had a minimum deviation of -1.31 nm and a maximum deviation of 1.6 nm for an average surface roughness of 561.43 pm across the film surface. The smooth polyimide films have less than 1% surface-roughness that shouldn't interfere with lithography, metal deposition, or etching in the fabrication process. Fig. 2 (E). depicts the distribution of surface roughness across 2 μm x 2 μm area of a 5 μm thick polyimide film.

G. Moisture Absorption

The absorption of water, which plasticizes the polyimide and compromises the insulation, is a major cause of failure for polyimide neural interfaces. A total of n=6 polyimide samples that were independently cured were tested for their moisture absorption values. Fig. 2 (F). shows a box plot of the distribution of the moisture absorption percentages of those films. From the values, we can surmise that the mean of the moisture uptake for n=6 polyimide films was around 1% when soaked for 24 hours in deionised water.

H. Microfabrication

Fig 3. shows the microfabricated depth array and surface μECoG array . The array thickness was measured using a surface profilometer (Dektak XT, Bruker) at 10.2 μm. After releasing the arrays off the silicon wafer in isopropanol, the devices were cleaned in Micro-90 (Cole-Palmer India) solution and rinsed with isopropanol and deionized water. The devices were then dried and tempered at 120°C for 6 hours on a hotplate. After tempering, the arrays were found to be completely straight and did not have any kinks in them. The arrays were then packaged by soldering the through-hole pads to an electronic interface board having 1.27 mm male pin headers.

I. Electrochemical Impedance Spectroscopy

A plot of the impedance values for n=5 surface arrays and n=5 depth arrays is shown in Fig. 3 (D) and Fig 3 (E). We characterize the electrode for its low frequency and 1 kHz impedances for LFP and single-unit analysis, respectively. According to the EIS phase plot, the electrode exhibits a dominant capacitive behavior at low frequencies and a resistive behavior at higher frequencies. An average impedance of 755kΩ was measured at 1 kHz for the depth probes, while the impedance of the surface μECoG arrays at 1 kHz was roughly 14 kΩ.

J. ISO-10993-11 Acute systemic toxicity testing

Polyimide extractions were administered to Swiss Albino Mice (N= 20, all Male, age = 6-7 weeks, weight = 18.91 - 20.69 gm) at a single dose of 50 mL/kg body weight intravenously for polar extractions and intraperitoneally for non-polar extractions. Throughout the monitoring period of 72 hours following treatment, they exhibited no adverse consequences (biological reactivity), body weight loss, or mortality. As a result, the tested Polyimide, was assessed to not induce any acute systemic toxicity and meet the test standards of ISO-10993-11. These tests were carried out at the RCC Labs, Hyderabad.

K. In vivo Neural Recordings

The unprocessed trace of neural activity from an example *in vivo* neural recording session is shown in Fig 4 (A). The raw data was processed offline in order to identify single units and local field potentials. Local field potentials were obtained by extracting the power in the 0.3-300 Hz frequency band. The time-frequency plot in Fig 4 (B), lower panel, displays the increase in broadband power (below 500 Hz) during spiking. The power in the 300–6000 Hz band for both the depth and μECoG probes was calculated in order to extract action potentials from the raw recordings. The action potentials were then divided into clusters that matched putative single units using Mountainsort5 [4]. One such isolated neuronal cluster from the sample session using μECoG probe is displayed in Fig. 4 (C). Similarly, clusters were isolated from the depth probes as well. For this session, a total of 3 clusters were isolated from the μECoG channels and 9 clusters were isolated from the depth probe as shown in Fig 5.

Next, we assessed and compared the signal quality of depth probes with that of μECoG array from 20 different epochs, each lasting 10 mins, from two animals. Following observations were made:

1. A higher number of neuronal clusters were isolated using the depth array (mean = 6.85, SEM = 1.546) compared to the μECoG array (mean = 3.66, SEM = 0.404), although the difference was not statistically significant (Fig 6 (A); Mann-Whitney U Test; p value = 2e-01).

2.The average SNR for depth probe across all sessions was significantly higher (mean = 3.77, SEM = 0.282) compared to that of μECoG (mean = 1.89, SEM =0.153) as shown in Fig 6 (B) (Mann-Whitney U Test; p value = 1.91e-06).

3. Recordings from μECoG clusters showed a greater average presence ratio (mean = 0.92, SEM = 0.027) implying the presence of a unit 92% of the recording. For depth probes, the presence ratio was significantly lower (mean = 0.58, SEM = 0.014; Mann-Whitney U Test; p value = 2.62e-12) as shown in Fig 6 (C).

4. Isolation distance between neuronal clusters was significantly higher for the depth array (mean = 22.52, SEM = 6.72) than that for the μECoG (mean = 17.89 , SEM = 3.33; Mann-Whitney U Test; p value = 1.94e-03) as shown in Fig 6 (D).

We also evaluated firing rates, Inter Spike Interval (ISI) violation ratio and the number of spikes recorded from the probes for each epoch but did not observe significant differences between the depth and surface arrays.

IV. Discussion

Our results on the synthesis and characterization of a clinical-grade polyamic acid and the microfabricated polyimide neural interfaces suggest that this technology can be an excellent candidate for acute neurosurgical intervention therapies. The depth and surface arrays were successfully able to record single unit and LFP activity, respectively, from the mouse model. Furthermore, our polyimide samples successfully cleared the acute systemic toxicity analyses performed as per ISO 10993-11 guidelines at an FDA-certified laboratory (RCC Labs, Hyderabad). For future work, long-term *in-vivo* behavior of the polyamic acid needs to be studied for its use as a stable, chronic neural interface material. Microfabrication of a higher channel count device will allow simultaneous mapping of multiple brain regions with a higher spatial resolution. The technology holds the potential for commercialization and use in the clinics for the development of brain-computer interfaces and invasive brain monitoring applications in epilepsy and other neurological conditions.

V. Acknowledgements

We would like to thank K. Nageswari and Deepti Rukade and the team at IIT Bombay Nanofabrication Facility for helping us coordinate our schedules for microfabrication. Our sincere thanks to Jamille Hetke and Rio Vetter at NeuroNexus Technologies for their guidance on the polyamic acid and polyimide electrode technology. We would like to thank Riddhi Bhalerao for assisting with the illustrations. Finally, we thank the staff at the Central Experimental Animal Facility at IIT Kanpur for their help and guidance on animal surgeries. Deepti Chugh and Garima Chauhan were supported by the Institute Postdoctoral Fellowship, IIT Kanpur. Kshitij Kumar was supported by ICMR-DHR-CoE. The study was funded by the Indian Council of Medical Research ITR grant and IIT Kanpur startup funds to Arjun Ramakrishnan.

VI. Declaration of interests

Kaustubh Deshpande and Arjun Ramakrishnan are co-founders of Eywa Neuro PLC. All the authors declare no competing interests.

VII. Author Contributions

KD and AR conceived the idea of the study. KD and NK designed and synthesised the polyimide and the neural probes. SG developed the transgenic mouse model used in the study. KK, GC, DC performed the animal surgery and data acquisition. KK analyzed the neural recordings. KD and KK wrote the original draft of the paper. All authors revised the manuscript.

References

1 Ainhoa Altuna, Javier Berganzo, and Luis J. Fernández. Polymer SU-8-based microprobes for neural recording and drug delivery. *Frontiers in Materials*, 2:53, 2015.

2 Elon Musk and. An integrated brain-machine interface platform with thousands of channels. *Journal of Medical Internet Research*, 21(10):e16194, October 2019.

3 Alessio Paolo Buccino, Cole Lincoln Hurwitz, Samuel Garcia, Jeremy Magland, Joshua H Siegle, Roger Hurwitz, and Matthias H Hennig. Spikeinterface, a unified framework for spike sorting. *Elife*, 9:e61834, 2020.

4 Jason E Chung, Jeremy F Magland, Alex H Barnett, Vanessa M Tolosa, Angela C Tooker, Kye Y Lee, Kedar G Shah, Sarah H Felix, Loren M Frank, and Leslie F Greengard. A fully automated approach to spike sorting. *Neuron*, 95(6):1381–1394, 2017.

5 Cristian P. Constantin, Magdalena Aflori, Rodica F. Damian, and Radu D. Rusu. Biocompatibility of polyimides: A mini-review. *Materials*, 12(19):3166, 2019.

6 Samira Diaham, Marie-Laure Locatelli, and Ramzi Khazak. BPDA-PDA polyimide: Synthesis, characterizations, aging and semiconductor device passivation. *High Performance Polymers - Polyimides Based - From Chemistry to Applications*, 2012.

7 Youngmi Ha, Moon-Chang Choi, Namjo Jo, Insu Kim, Chang-Sik Ha, Dongwook Han, Sungwoo Han, and Myungbeom Han. Polyimide multilayer thin films prepared via spin coating from poly(amic acid) and poly(amic acid) ammonium salt. *Macromolecular Research*, 16(8):725–733, 2008.

8 C. Hassler, T. Boretius, and T. Stieglitz. Polymers for neural implants. *Journal of Polymer Science Part B: Polymer Physics*, 49(1):18–33, 2010.

9 D. N. Hill, S. B. Mehta, and D. Kleinfeld. Quality metrics to accompany spike sorting of extracellular signals. *Journal of Neuroscience*, 31(24):8699–8705, June 2011.

10 Alexander Kullmann, David Kridner, Sean Mertens, Mark Christianson, Delphine Rosa, and Camilo A. Diaz-Botia. First food and drug administration cleared thin-film electrode for intracranial stimulation, recording, and monitoring of brain activity—part 1: Biocompatibility testing. *Frontiers in Neuroscience*, 16:903650, 2022.

11 Sung Eun Lee, Sang Beom Jun, Hyun Joo Lee, Jinhyung Kim, Seung Woo Lee, Changkyun Im, Hyung-Cheul Shin, Jin Woo Chang, and Sung June Kim. A flexible depth probe using liquid crystal polymer. *IEEE Transactions on Biomedical Engineering*, 59(7):2085–2094, 2012.

12 Yuan Liu, Jia Liu, Shizhe Chen, Ting Lei, Youngjun Kim, Simiao Niu, Hongbo Wang, Xinge Wang, Amir M. Foudeh, Jeffrey B.-H. Tok, and Zhenan Bao. Soft and elastic hydrogel-based microelectronics for localized low-voltage neuromodulation. *Nature Biomedical Engineering*, 3(1):58–68, 2019.

13 Miguel A. L. Nicolelis, Asif A. Ghazanfar, Barry M. Faggin, Steven Votaw, and Luiz M. O. Oliveira. Reconstructing the engram: Simultaneous, multisite, many single neuron recordings. *Neuron*, 18(4):529–537, 1997.

14 Arto Nurmikko. Challenges for large-scale cortical interfaces. *Neuron*, 108(2):259–269, October 2020.

15 Juan Ordonez, Markus Schuettler, Clemens Boehler, Timo Boretius, and Thomas Stieglitz. Thin films and microelectrode arrays for neuroprosthetics. *MRS Bulletin*, 37(6):590–598, 2012.

16 A. R. Preston and H. Eichenbaum. Interplay of hippocampus and prefrontal cortex in memory. *Current Biology*, 23(17):R764–R773, 2013.

17 Burga Rubehn and Thomas Stieglitz. In vitro evaluation of the long-term stability of polyimide as a material for neural implants. *Biomaterials*, 31(13):3449–3458, 2010.

18 John P. Seymour and Daryl R. Kipke. Fabrication of polymer neural probes with sub-cellular features for reduced tissue encapsulation. *2006 International Conference of the IEEE Engineering in Medicine and Biology Society*, 2006.

19 John P. Seymour, Fuxi Wu, Kensall D. Wise, and Euisik Yoon. State-of-the-art MEMS and microsystem tools for brain research. *Microsystems & Nanoengineering*, 3(1):17066, 2017.

20 Carson S. Smith, Daniel W. Scott, Michael H. Kim, L. Douglas Sanford, Kyoungho D. Song, and Hyungil Yoon. Polyimide neural probe for chronic sensing of neural activity and micro-positioning. *SPIE Proceedings*, 2013.

21 Xinyi Wang, Aaron W. Hirschberg, Haifeng Xu, Zane Slingsby-Smith, Anna Lecomte, Kevin Scholten, Dan Song, and Ellis Meng. A Parylene neural probe array for multi-region deep brain recordings. *Journal of Microelectromechanical Systems*, 29(4):499–513, 2020.

22 S. M. Wellman, J. R. Eles, K. A. Ludwig, J. P. Seymour, N. J. Michelson, W. E. McFadden, A. L. Vazquez, and T. D. Y. Kozai. A materials roadmap to functional neural interface design. *Advanced Functional Materials*, 28(12):1701269, 2017.

23 Alon Weltman, Jaeseok Yoo, and Ellis Meng. Flexible, penetrating brain probes enabled by advances in polymer microfabrication. *Micromachines*, 7(10):180, 2016.

24 Wen Yang, Fei Liu, Hong Chen, Xiaolin Dai, Wenbin Liu, Xiaolin Qiu, and Xu Ji. Influence of heating rate on the structure and mechanical properties of aromatic BPDA-PDA polyimide fiber. *Polymers*, 12(3):510, 2020.

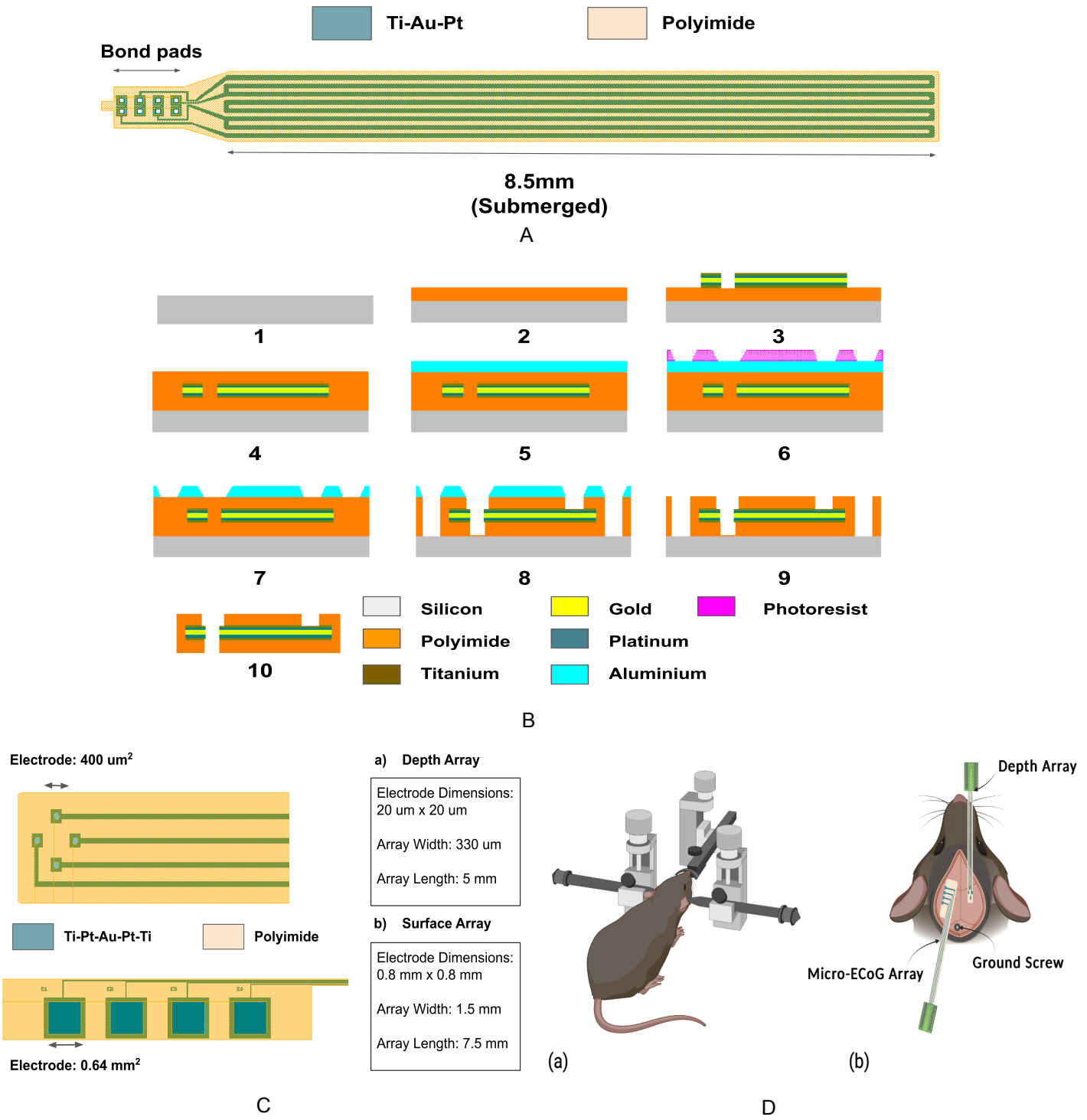

Fig 1. (A) Shows a test structure for corrosion testing of the polyimide. An 8.5 mm long gold channel arranged in a serpentine manner was encapsulated in 5um polyimide. EIS analysis was performed in PBS 1X and the impedance of the test structure was measured to determine whether or not the polyimide thin film was compromised.
(B) Polyimide MEA Microfabrication Process Steps 1) RCA clean silicon wafer 2) Spin coat and cure a base layer of polyimide 3) Liftoff Ti-Pt-Au-Pt-Ti channels 4) Spin coat and cure a second layer of polyimide 5) Evaporate 100 nm Al film 6) Pattern photoresist over Al layer 7) Wet etch Al layer to make the hard mask for subsequent polyimide etching 8) O2 plasma etching of polyimide to define outline, electrodes and bond pads 9)Blanket wet etching of Al hard mask 10) Release in IPA.
(C) Illustrative representation of the depth and surface µECoG neural arrays design.
(D) (a) Illustrative representation of anesthetised mouse on the stereotactic system. (b)Illustrative representation of the placement of the depth and surface µECoG neural arrays.

A

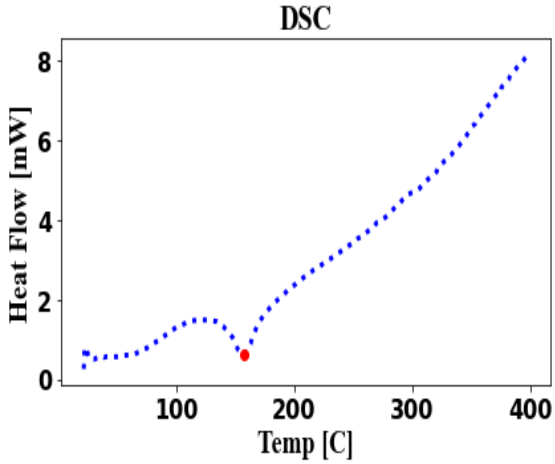

B

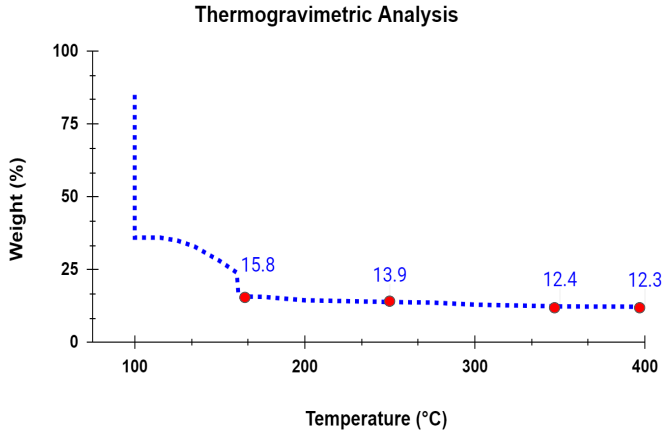

C

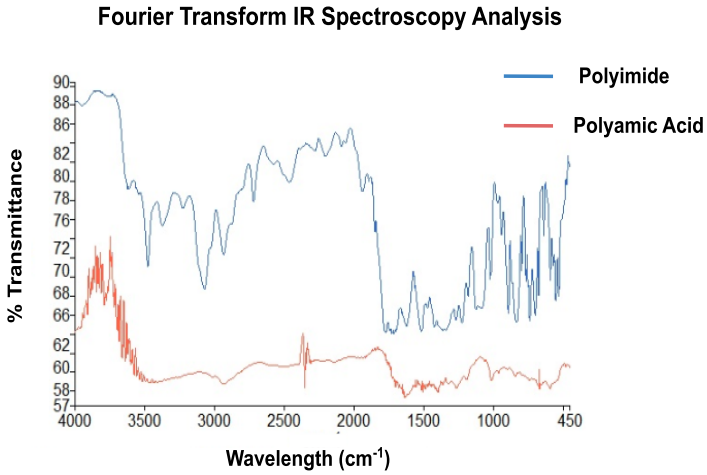

D

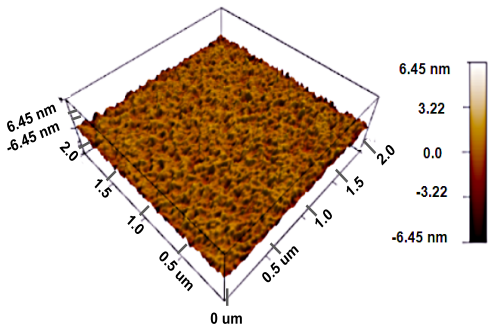

E

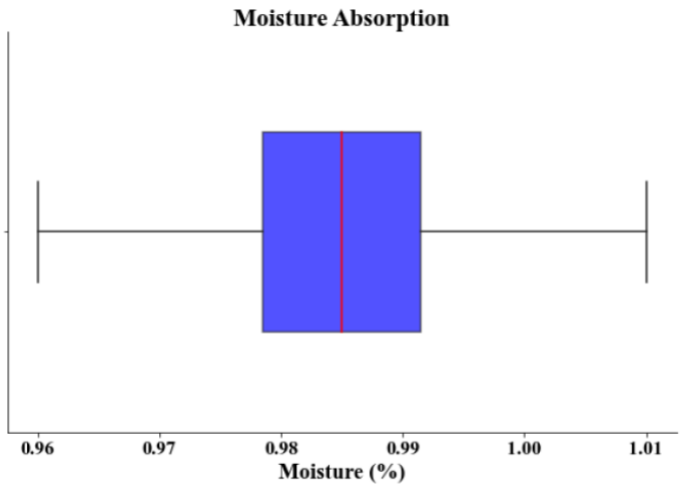

F

Fig 2. (A) Polyamic acid was spin-coated on 50mm silicon wafers and soft-baked on a hotplate at 100°C for 5 minutes followed by 120°C for 5 minutes. The spun wafers were then inspected under high magnification on an optical microscope for the presence of any pinholes or particles.
(B) DSC Exotherm on a polyamic sample showing non-reversing heat flow behaviour with only a single transition change at 160°C. The temperature was ramped from 75°C to 400°C at 10°C/min. (C) TGA Analysis of the polyamic acid shows the % of weight loss in the polyamic acid sample as it is cured from 75°C to 400°C. Most of the weight loss occurs by 160°C which is the evaporation point of the DMAc solvent. Imdization and subsequent loss of H2O continues up to 400°C with most of the imidization completed by 350°C
(D) Shows the FTIR spectra for the Polyimide and the polyamic acid.
(E) Surface roughness distribution of a 2mm x 2mm Polyimide film having a film thickness of 5um measured using atomic force microscopy. The average surface roughness was around 0.5nm and the roughness was fairly uniform across the whole cross-section.
(F) Box plot showing the moisture absorption ratio of n = 6 samples with a mean percentage of 0.984 and standard deviation of 0.016.

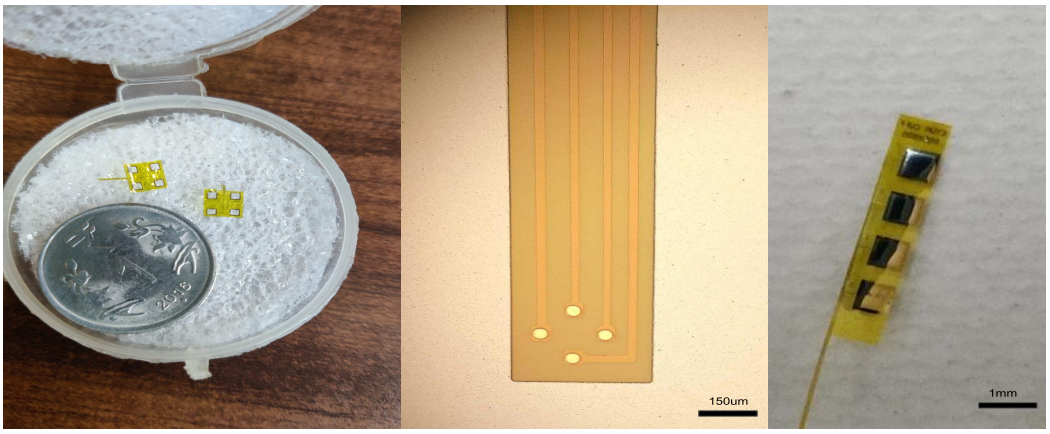

A B C

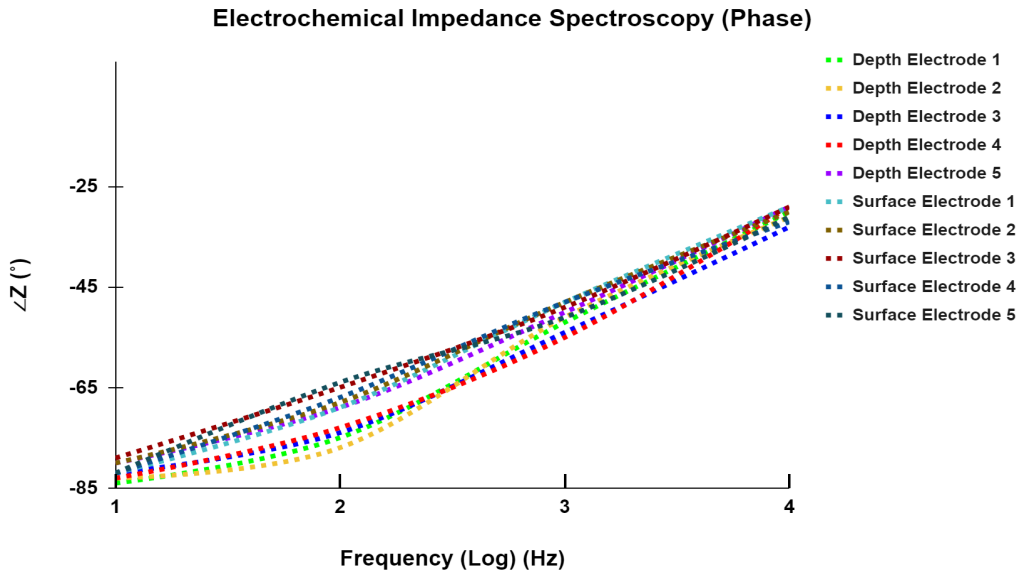

D

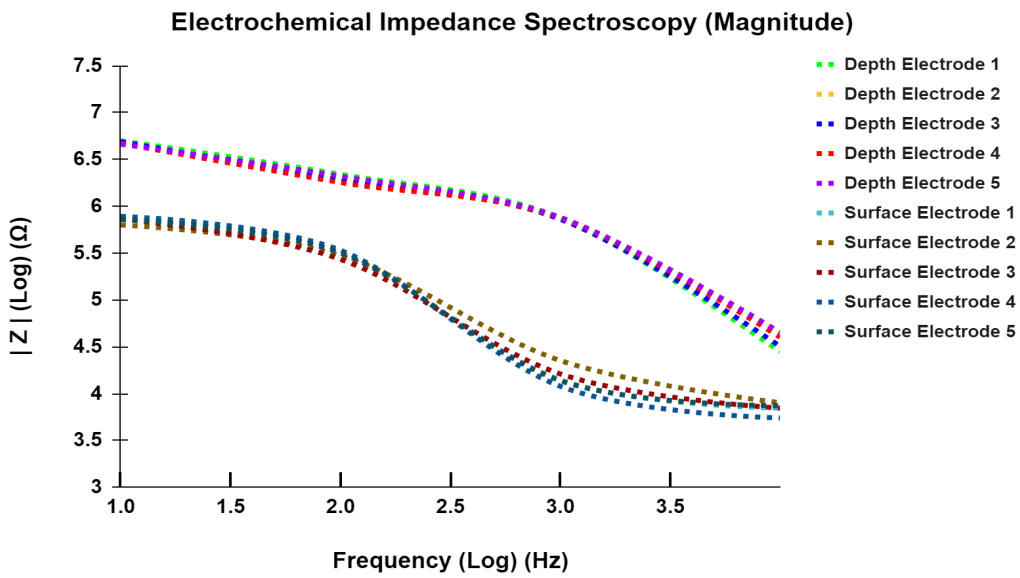

E

Fig 3. (A) Depth arrays next to a 1 Indian Rupee coin.
(B) Depth array electrodes under an optical microscope.
(C) Tempered surface of µECoG array.
(D) Shows the EIS Impedance phase spectrum between 100Hz to 10kHz for a depth and surface µECoG array.
(E) Shows the EIS Impedance magnitude spectrum between 100Hz to 10kHz for a depth and surface µECoG array.

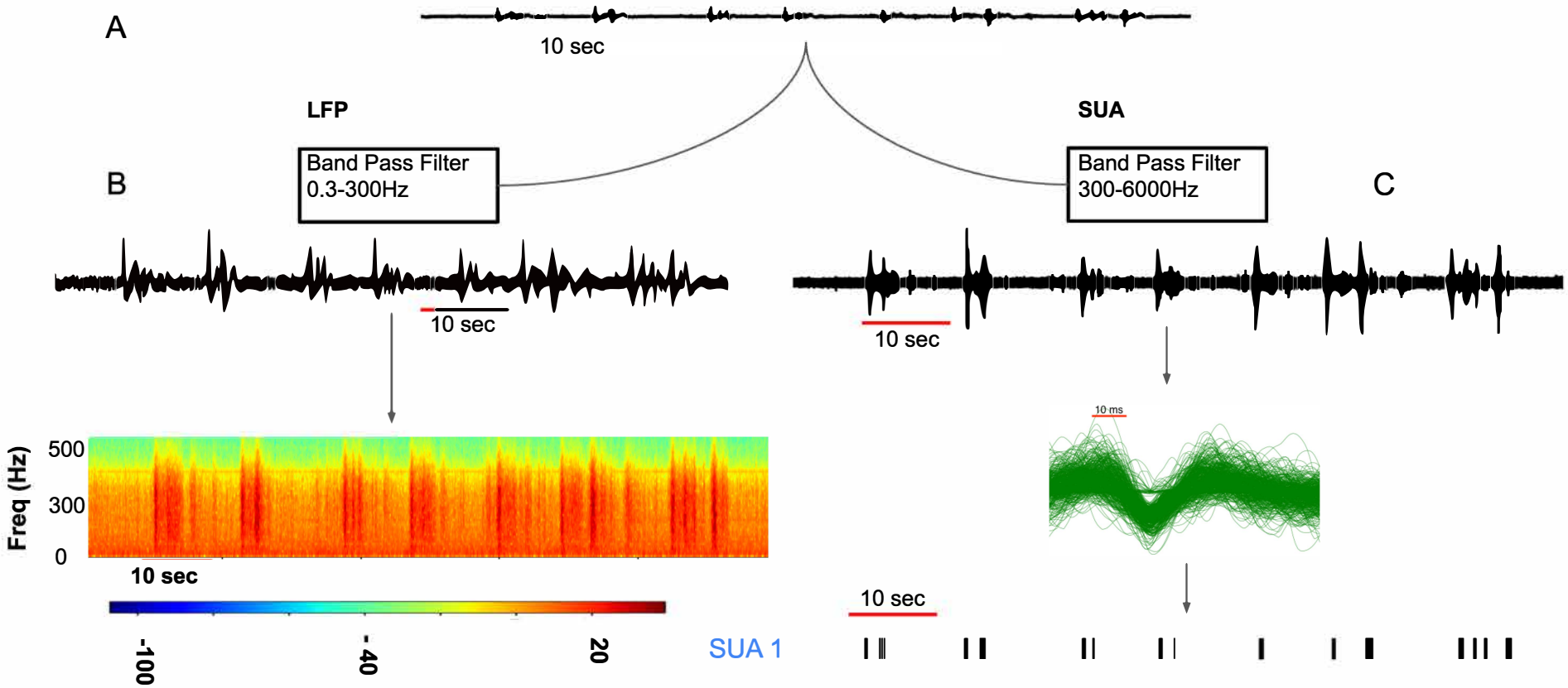

Fig 4 (A) Raw unfiltered neural data (B) Local field potentials and the associated time-frequency plot. (C) Single Unit activity (SUA). Below: waveform and raster plot for the spiking activity for one cluster from a depth array.

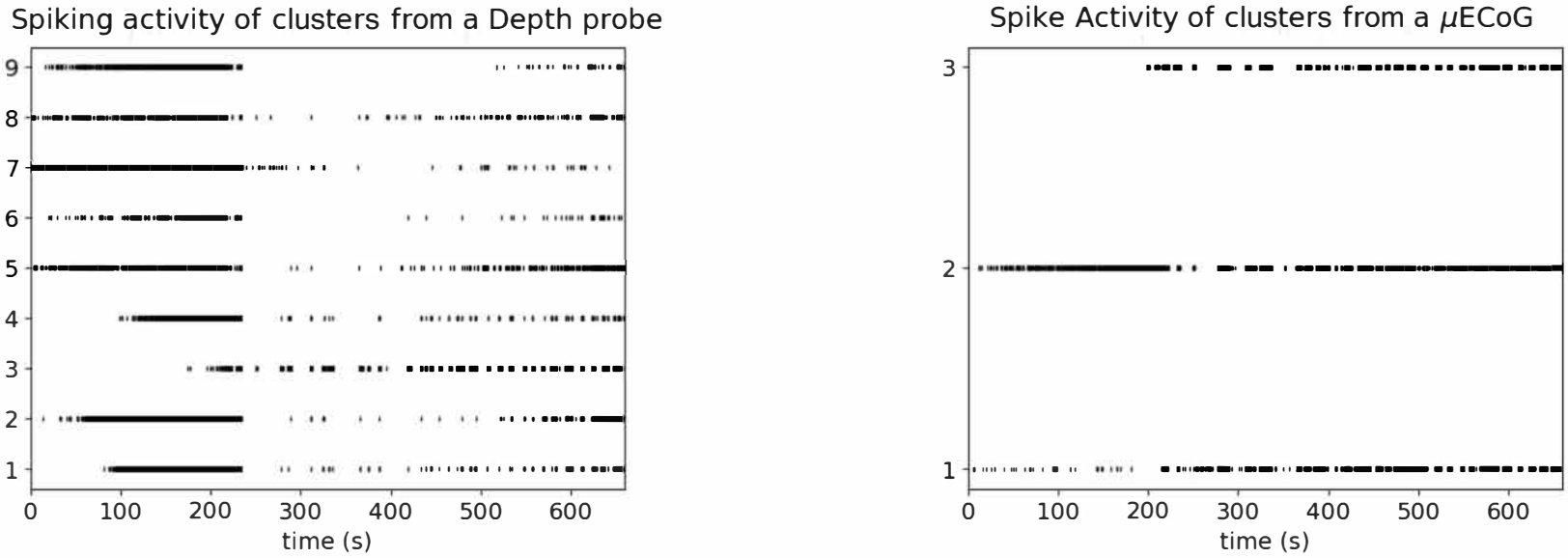

Fig 5 (A) Shows neural clusters from a sample session recorded from the depth array. 9 clusters were identified. (B) Shows neural clusters form the sample session recorded using a μECoG array. 3 clusters were identified.

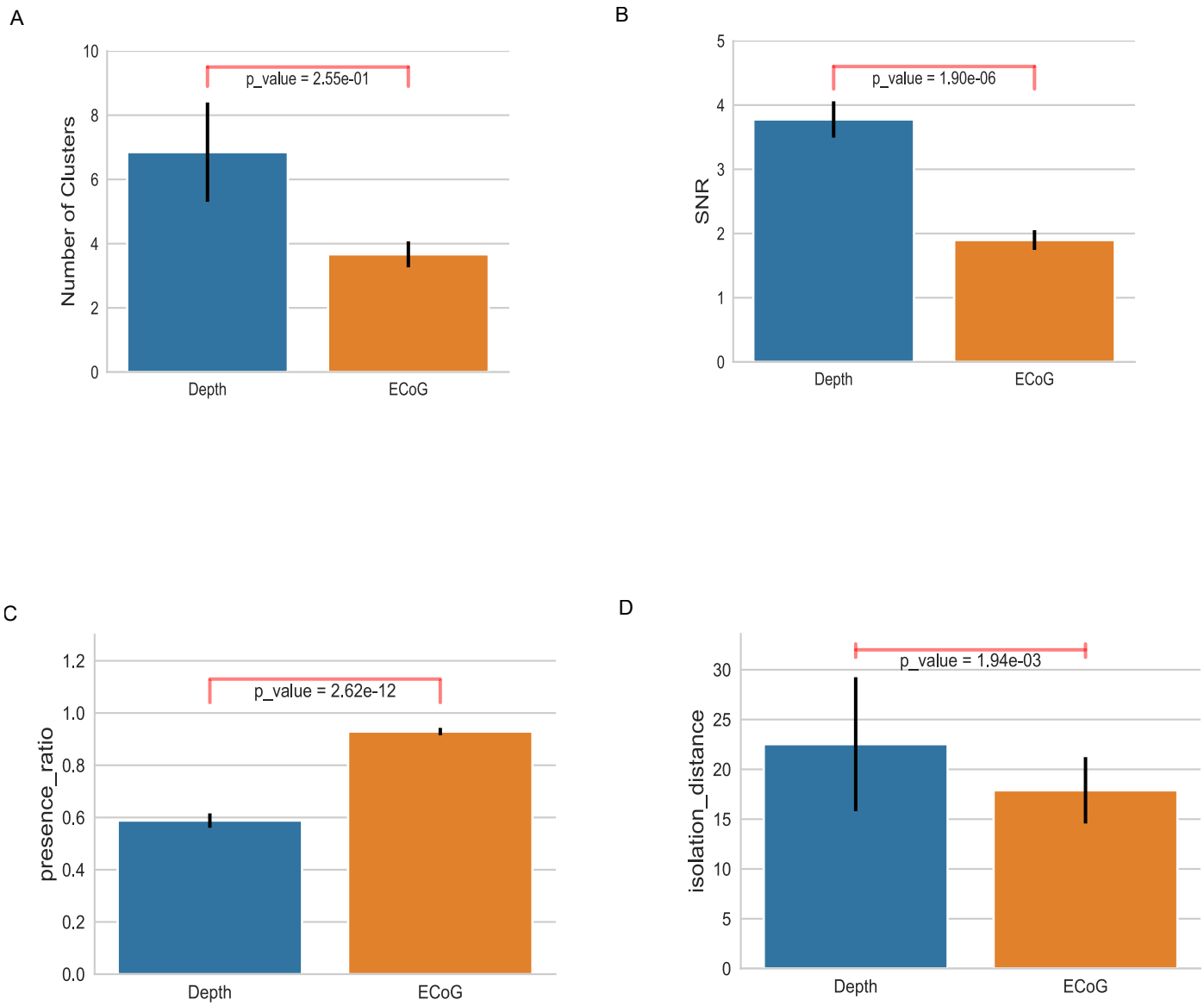

Fig 6 (A) Shows distribution of the Neural Clusters across all sessions recorded from the arrays.
(B) Shows SNR for all the sessions from the different probes.
(C) Shows the distribution of the presence ratio of the probes.
(D) Shows the distribution of the isolation distance across the sessions.